Available online at www.sciencedirect.com

ScienceDirect

Procedia Manufacturing 34 (2019) 655–665

Procedia MANUFACTURING

www.elsevier.com/locate/procedia

47th SME North American Manufacturing Research Conference, Penn State Behrend Erie, Pennsylvania, 2019

Design of Functionally Graded Lattice Structures using B-splines for Additive Manufacturing

Archak Goel[a], Sam Anand[b]*

[a,b] *Center for Global Design and Manufacturing*
Department of Mechanical & Materials Engineering, University of Cincinnati, Cincinnati, OH 45221, USA

* Corresponding author. Tel.: +1-513-382-5236; *E-mail address:* anands@ucmail.uc.edu

Abstract

Additive manufacturing methods have recently been used to make light-weight parts using lattice structures for various applications. Functionally graded lattice structures (FGLs) are structures that are designed using lattices with a varying distribution of porosity by virtue of varying the volume fractions of each unit cell in the 3D design domain. This graded design helps to achieve advanced properties related to structural strength, allow functionalities such as bone ingrowth and optimum heat transfer etc. Compliance minimization is one such classic problem where topology optimization techniques are used to determine the optimum distribution of material in the design domain while obtaining the desired reduction in weight. This material distribution is typically populated with lattices of variable volume fraction unit cells to generate FGLs. Truss type unit cells such as BCC are commonly used to develop FGLs. To develop such structures with truss type unit cells there is a need for a methodology that can maintain smooth connectivity among unit cells of varying densities. This paper discusses a new method to achieve smoothly connected FGLs, based on a BCC unit cell geometry, using a B-spline surface-based unit cell design methodology. The lead author's previous work in [1] on generating bifurcating geometries using B-spline surfaces is extended to lattices as a case of multi-furcation geometries. First, a control polyhedron net is developed on the basis of desired unit cell geometry which is then further processed to construct water-tight boundary representation of the unit cell using a 3rd order B-spline surface. This design methodology is used in conjunction with an algorithm to populate the density distribution from SIMP based topology optimization using unit cells with different volume fractions. The resulting lattice structure is compared with a uniform density lattice structure of similar light-weighting. It is shown that the methodology discussed in this paper could be successfully used to construct FGLs with high stiffness.

Keywords: graded lattice/cellular/porous structures, B-splines, Additive Manufacturing/3D Printing

1. Introduction

Additive manufacturing methods are being extensively used for developing intricate geometries that are lightweight for fulfilling advance functional requirements. Due to the layer-wise fabrication methodology, structures with highly complex geometries can be manufactured that are difficult or impossible to manufacture with conventional manufacturing methods. Lattice structures are one such type of geometries, consisting of an arrangement of partially filled unit cells. Repeating one of such unit cells type in a uniform manner in a design domain generates periodic lattice structures. However, when this distribution is graded in an optimized fashion by varying the unit cell's geometric parameters such as porosity (volume

10.1016/j.promfg.2019.06.193

fraction) a functionally graded lattice structure (FGL) is obtained. FGLs help achieve advanced functional properties while minimizing the overall weight of the part. For example, bones have a graded porous structure and graded lattice structures are used for mimicking the original bone structure to design medical implants [2]. This design strategy helps to fulfill the complex structural as well as critical functional requirements of the bone such as facilitating bone-in-growth through the interconnected porous network [2, 3]. Similarly, porosity distribution in an optimized manner can be extremely useful to develop light-weighted multi-functional structures. In prior work, [4] developed an equation for specific thermal conductivity in terms of geometric parameters of the unit cell geometry. On the basis of such studies, by controlling the geometric parameters of unit cells, light-weighted structures could be optimized for stiffness using a graded distribution of lattices while meeting functional goals such as convective heat transfer.

FGLs have also shown superior performance for structural applications such as high stiffness [5] and energy absorption [6] in comparison to their uniform density counterparts. For optimizing structural performance, FGLs are most commonly designed using topology optimization techniques. Topology optimization algorithms such as [7] output a voxelized domain with varying material density values in each voxel that are correlated to geometric parameters of a lattice such as strut thickness or porosity leading to a graded structure. The graded structure thus obtained helps attain maximum structural stiffness.

Amongst various types of lattices, strut type lattices such as Body Centered Cubic (BCC) are a popular choice across the entire spectrum of above mentioned application domain [3, 4, 6, 8]. Particularly for structural optimization, strut thicknesses are varied to control porosity of such geometries while populating lattices as per the topology optimization density output. This leads to a design issue of establishing connectivity at corners of each voxel where struts of multiple diameters merge [9]. Lack of connectivity leads to inconsistent designs that do not perform optimally for fulfilling mechanical loading requirements [2]. As a workaround to this issue, recent works have used alternate unit cell geometries such as gyroids [9] or shwartz diamond [2] to construct FGLs.

In this paper, a new B-spline surface-based design representation for strut type unit cell is discussed that generates smooth strut-strut interaction boundaries in each cell as well as allows local shape modification to facilitate smooth connectivity at junctions of struts of different diameters in FGLs. B-spline surfaces are also advantageous since a B-spline based design tool is readily integrable as a new tool within a CAD solid modelling environment. NURBS is a common framework used in CAD software packages for representing shape boundaries and B-splines are essentially NURBS with weights set to 1. Moreover, in comparison to the other popular surface generation methods used for lattices – implicit surfaces where additional operations are required to generate and smoothen the mesh, meshing is almost automatic in B-spline surfaces. The property of B-spline surfaces that allow to modify the shape locally, makes this tool a precursor to develop fully Design for Additive Manufacturing (DFAM) compliant lattice structures. For example, in a typical Direct Metal Laser Sintering (DMLS) process, unit cells in a lattice structure with large overhangs will need support structures to build them. Removing those supports could be very difficult or impossible due to the geometric complexity of the lattice structure. Other phenomenon such as oversizing of struts or blockage of small openings at the joints by the excess sintered powder can lead to closing of the intended open porous structure and addition of unwanted weight to the structure. These problems could also affect the mechanical performance of the manufactured structure. Using B-splines, the existing lattice geometry could be morphed locally by setting the control points of the surface to develop designs with compensated strut diameters, support-free arched overhangs and minimum small openings. These advantages also make using B-splines a very promising tool to develop lattice structures in the future that are DFAM compliant.

Developing unit cells geometries with B-splines surfaces could be a complex problem due to the possible surface intersections [10]. The lead author's previous work in [1] on generating bifurcating geometries using B-spline surfaces is extended to lattices as a case of multi-furcation geometries. The methodology is implemented for the case of a BCC unit cell which is quite widely used. First, an appropriate control polyhedron is generated based on unit cell's geometric parameters such as strut diameter, strut angle and cell size. Thereafter, a water-tight boundary representation is constructed for each unit cell using a 3rd order B-spline surface.

This new representation scheme is used to generate smoothly connected FGLs using outputs from a SIMP (Solid Isotropic Material with Penalization) based topology optimization algorithm by [7] for the case of a cantilever beam. The entire methodology for constructing FGLs is incorporated as custom functions in SIEMENS NX solid modeling environment using its NX Open programming environment. Two examples are discussed where FGLs are constructed and compared with their uniform density counterparts of similar light-weighting for minimum stiffness criteria using FEA. The results confirm that methodology can be used to develop FGLs with high performance.

2. Literature review

This section focuses on relevant literature on unit cell design methods, FGLs and topology optimization schemes.

2.1. Unit cell design methods

Several different approaches for unit cell design has been discussed in literature. An STL surface representation of a unit cell was developed in [11]. To obtain the surface of struts, they used ACIS solid modeler to create solid struts first followed by end face removal of each strut. The method was improved in [12] to directly create a surface mesh, enable variable cross-sections struts and filleted strut intersections. However, both of the methods required additional Boolean operations to add spheres or fillets at the strut intersections in each unit cell. A simpler method discussed in [13] involved creating polygonal strut profile-based cell library using hollow struts. All these

methods required additional and complex operations to make a watertight unit cell surface. A Catmull-Clark based surface subdivision scheme to generate smooth mesh models of strut type lattices was discussed in [14]. Their method requires multiple iterations and its usability to generate a 3D graded lattice structure was not discussed. A B-spline based irregular 2D porous structure generation scheme was discussed in [15].

Another approach to design lattice structures for AM is using implicit surfaces [16]. Gyroids are one of the popular unit cell types represented by this method. In this method, a limited range of gyroid based unit cells can only be represented using their corresponding pre-defined mathematical equations. There is some flexibility to alter the unit cell by only adjusting the volume fraction and cell size [9, 17]. A discrete signed distance field implicit representation was used in [10] to generate template-based unit cells. In all the implicit surface representation methods, obtaining the actual surface mesh and smoothening it requires several additional complex computational steps. Among the recent approaches to design FGLs, conventional primitive based strut type unit cell representations are used along with appropriate Boolean operations by [8, 18] and a polygonal type strut representation scheme for a direct STL file generation was used by [3]. Both schemes suffer from the issue of unwanted sharp edges along the struts and at the strut intersections.

2.2. FGL design and analysis

There are many efforts towards developing FGLs using AM. Panesar et al. developed uniform and graded lattice structures in [8] made of different unit cell types – gyroids and BCC and concluded that FGLs as a more robust strategy for mechanical performance in comparison to uniform lattice structures. Maskery et al. studied graded BCC lattice structures under compressive loading in [8] and reported that FGLs can be used for tailored response to compressive loads. FGLs were manufactured using SLM and studied for their mechanical properties for bone implant applications by [2]. They showed that mechanical properties such as elastic modulus and yield strength can be tailored by adjusting the gradation of porosity and established a mathematical relationship between the mechanical parameters and porosity. A voxel-based method of generating unit cells for conformal FGLs was developed by [19]. They used an 8-bit grayscale bitmap to generate gradations in strut diameter.

2.3. Topology optimization

Topology optimization is quite commonly used to populate a design domain with lattice structures. Topology optimization was first introduced by [20] and further developed into a SIMP based scheme in [21] where the intermediate densities are represented using a penalization based power law approach. SIMP based topology optimization with lattices has been used to generate FGLs by [8, 9]. [7] developed an efficient MATLAB based code for solving topology optimization problems that was used in this paper.

3. Methodology

The methodology to design BCC unit cell design using B-splines surfaces and then using those cells to develop FGLs in conjunction with a SIMP based topology optimization output is discussed in this section. The nomenclature used is detailed below:

Nomenclature

L	Length of a unit cell
W	Width of a unit cell
H	Height of a unit cell
D	Strut diameter
P	Number of sides of a regular polygon
Φ	Interior angle of a regular polygon
T_1	Perpendicular distance of the start pt. of strut skeletal curve from central reference axis
T_2	Perpendicular distance of the end point of the strut skeletal curve from the central reference axis
T_3	Minimum distance between last strut polygons of top and bottom struts in a unit cell
S	B-spline surface
u,v	Parametric inputs of a B-spline surface
k	Degree of B-spline surface along parameter u
l	Degree of B-spline surface along parameter v
B	Control polyhedron matrix for a B-spline surface
m	Row size of B is equal to m+1
n	Column size of B is equal to n+1
N	B-spline surface basis functions along parameter *u*
M	B-spline surface basis functions along parameter *v*

3.1. Unit cell design

Each unit cell occupies a voxel and a periodic arrangement of all such voxels in 3D generates the whole lattice structure. In this work, the unit cell is modelled by using a water-tight B-spline boundary surface. Its geometric parameters are cell size, strut diameter and strut angle which are constrained for the case of a BCC such that length, width and height are equal and strut angle from horizontal always equals to 35.26° as shown in Fig. 1(a). The strut diameter is set as a variable and is proportional to the desired volume fraction. Based on these variables, first a set of parametric skeletal curves of the unit cell are generated which in turn are used to sweep out polygonal sections at uniform parametric intervals along the curves (Fig. 1(b)). These sections are required to develop a 3D control polyhedron for interpolating a B-spline surface.

In a BCC geometry, 8 struts meet at a common node, some previous efforts for modeling such lattice geometries have reported complexity in handling surface/mesh generation at the node area [11, 13]. This geometric problem is somewhat similar to the case of bi-furcating surfaces where two surfaces separate out from a single surface (Fig. 2(a)). However, in the case of a BCC, it is a multi-furcating geometry as shown in Fig. 2(b). The

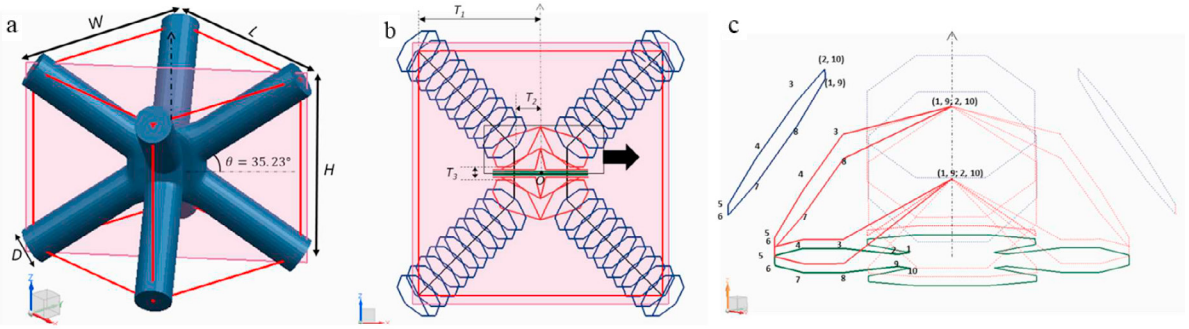

Fig. 1. (a) Input geometric parameters for a unit cell and a BCC geometry as constructed using B-spline surfaces in this work. The body diagonal plane is also shown; (b) control polygons, skeletal curves in black, central reference axis and distances as seen in the body diagonal plane. Polygons in blue are strut polygons, in red are special polygons and in green are stem polygons. (c) arrangement of control points.

intersection region separate out into 4 struts at the top and 4 at the bottom. Surface modelling of such furcating geometries is a complex geometric problem and often involves several steps to perform hole-filling operations while maintaining continuity especially at the furcation region [1]. In a lattice structure there are numerous repetitions of a unit cell geometry which makes it highly undesirable to have such extra hole-filling operations. In order to avoid these extra steps, lead author's previous work [1] on reconstruction of bi-furcating (one stem to two branches) geometries is extended in this paper for the case of multi-furcating (one to many branches) geometries. A scheme is developed for obtaining the arrangement of control points for modelling the multi-furcating surface using B-splines without the need for any hole-filling operations. The algorithms for generating skeletal curves, polygonal sections and control point arrangement are discussed in the subsequent subsections. The B-spline surface is reconstructed using the following equation from [22]:

$$S(u,v) = \sum_{i=1}^{(n+1)} \sum_{j=1}^{(m+1)} B_{(i,j)} N_{(i,k)}(u) M_{(j,l)}(v) \quad (1)$$

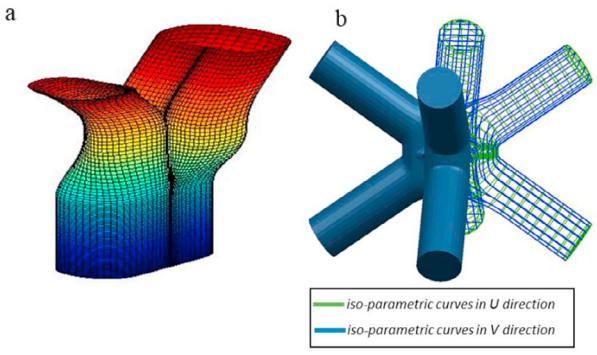

Fig. 2. (a) Bifurcating surface geometry from [10] – a single stem diverging into two branches. (b) multi-furcating BCC geometry. Solid struts and iso-parametric B-spline surface curves are shown.

The surface is 3rd order in both parametric directions - u and v with uniform and periodic knots respectively. The surface curves in both the parametric directions for a BCC unit cell are shown in Fig. 2(b). The higher the order of the surface, the higher is the continuity that can be achieved. An order of 3 is sufficient to attain C^1 or G^1 continuity.

3.1.1. Algorithm for defining skeletal curves

The centroid of voxel (O) is the origin for calculations of distances of all parametric features for each unit cell, and the central axis passing through the origin and parallel to height of the voxel is the reference central axis as shown in Fig. 1(b). The skeletal curves for the struts are defined in the form of parametric lines such that their starting points are corners of the voxel inclined at an angle of 35.26º towards the center or origin of the voxel. The end points of the lines are calculated based on strut diameter such that the adjacent struts do not intersect. The distances of start and end points from central axis are summarized by following formulae:

$$T_1 = \mathrm{L}/\sqrt{2} \quad (2)$$
$$T_2 = (D * 0.5)/\cos(\emptyset/2) \quad (3)$$
$$T_3 = H - ((2\tan\emptyset) * (T_1 - T_2)) - D\cos\emptyset \quad (4)$$

A second set of parametric lines for constructing the node region of the lattice are defined as shown in Fig. 1(b). They start from the end points of top strut skeletal curves in a direction parallel to the central axis and end at the end points of bottom set of strut skeletal curves.

3.1.2. Methodology for defining sections

First, the stacking of control polygons is explained, thereafter the relative arrangement of control points is discussed in the context of modeling a multi-furcating BCC geometry.

There are 3 major type of polygons for each unit cell – strut polygons, special polygons and stem polygons as shown in Fig. 1(c). Strut polygons define strut geometry, special polygons are used to handle the transition of topology from four separate surfaces of struts to a single surface in the stem region and stem polygons define the node region where all 8 struts meet. Strut polygons can be any 'P' sided regular polygon having an in-circle diameter equal to the strut diameter. They are swept along the strut curves at parametric intervals such that their centroids lie on the strut curve. The plane containing each

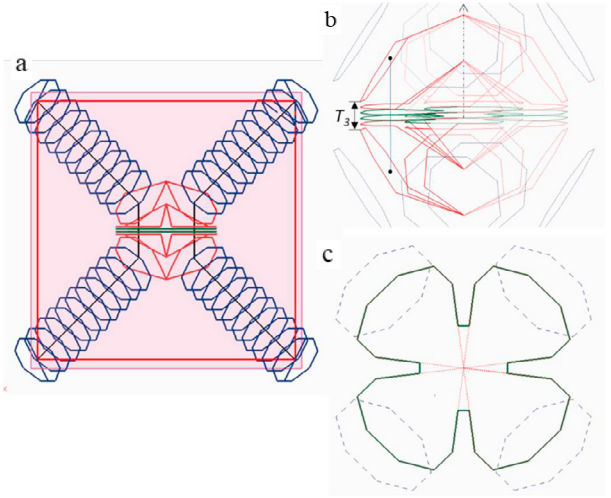

Fig. 3. Enlarged view of control polygons at the intersection region and formation of stem polygon geometry. (a) control polygons as viewed in the body diagonal plane. (b) enlarged front view of the intersection region in (a), showing the gap between 1st special sections of top and bottom set of struts as T_3. (c) geometry of stem polygons in top view of (a). Stem polygons are shown with solid lines, special and strut polygons are shown with dashed and dotted lines respectively.

polygon is perpendicular to the axis of the strut so that when the strut is sliced in that plane, a circular cross-section is obtained just like in a conventional BCC geometry. Based on the design guidelines discussed in [1] for furcating geometries, a total of 2 special sections are used. The 1st special section is defined at the last point on the strut curves. The 2nd special section followed by stem polygons are arranged in an equally spaced manner, in the gap between the 1st special sections of the top and bottom pair of struts polygons as shown in Fig. 3(a). The gap, T_3 could be determined from Eq. 3. After the stem polygons, the arrangement of special and strut polygons are repeated for the lower half of the BCC.

3.1.3. Orientation and arrangement of points

Points in all the polygons follow the arrangement as shown in Fig. 1(c). The set of polygons at each parametric step along the skeletal curves comprise of one row of the input control polyhedron matrix (Eq. 5). The total number of rows are equal to the total number of such parametric intervals at which polygons are created, including strut, special and stem polygons. The numbers indicated on the polygon vertices in Fig. 1(c) correspond to their respective column positions in the corresponding row vector of the control points matrix $\boldsymbol{B}$ from Eq. 1. The matrix is expanded below:

$$B_{i,j} = \begin{bmatrix} 1 & \cdots & 4*(P+2) \\ \vdots & \ddots & \vdots \\ n+1 & \cdots & 4*(P+2) \end{bmatrix} \quad (5)$$

such that,

$$4*(P+2) = m+1 \quad (6)$$

In the strut polygons, the first two points are repeated at the last to get an overlapping edge. This feature enables a smoothly wrapped surface curve throughout the strut length. Therefore, in Eq. 5, the total number of columns in $\boldsymbol{B}$ is equal to the summation of repeated polygon vertices of all 4 struts. The geometric arrangement of vertices of the special polygons is slightly different from the strut polygons except that one of their segments is of zero length. In other words, a pair of vertex locations are coincident. They are also constrained to lie on the voxel's central axis so that the coincident vertices of all special sections are bound to be coinciding as well. It ensures connectivity of surfaces as they transition from disjoint strut surfaces to the stem region.

Each stem polygon is made of four open polygons which collectively make a closed polygon geometry as shown in Fig. 3(b). They are generated by projecting all but coinciding vertices of special polygons on the plane perpendicular to the central reference axis of the voxel. Hence, they inherit the same base geometry of a regular polygon but with a different set of starting and trailing edges. These starting and trailing edges of each constitutive open polygon are overlapping with adjacent open polygons. Using this method, upon interpolation of the surface contours, tangent continuity is maintained near this region resulting in a smoother intersection zone. Overall, this arrangement of control points for all 3 type of polygons discussed also ensures that the surface is symmetric with respect to the central axis and with surface elements of minimum twist.

In order to ensure a water-tight surface representation, the open ends of the struts are closed by using two additional "sandwich" polygons at each strut as shown in Fig. 4. For constraining the end faces to be planar, two sections of regular polygons are made co-planar having their centroids co-incident with the sandwiched polygons.

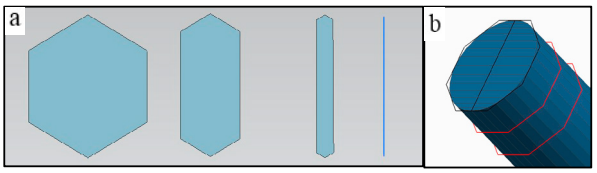

Fig. 4. (a) Illustration of sandwiched polygon and (b) highlighting the position of sandwiched sections along with the 1st two coplanar strut polygons.

3.2. Generating FGLs

A typical process to generate FGLs is shown in the flow chart in Fig. 5. Topology optimization algorithms are commonly used to obtain an optimum material distribution for a given light-weighting criteria while maximizing structural performance. The voxelized density distribution as obtained from the topology optimization algorithm is populated with the unit cells designed using methodology discussed in previous sections. In this paper a SIMP based topology optimization scheme is used as proposed in [7]. It generates density values ranging from 0 to 1 in each voxel of a 3D voxelized domain. It also employs a penalization scheme to skew fractional values towards either 0 or 1. Since the entire FGL is constructed for a single material in this work, the partial density values from topology optimization algorithms is considered equivalent to a parameter called the volume fraction of a unit cell. It is the ratio

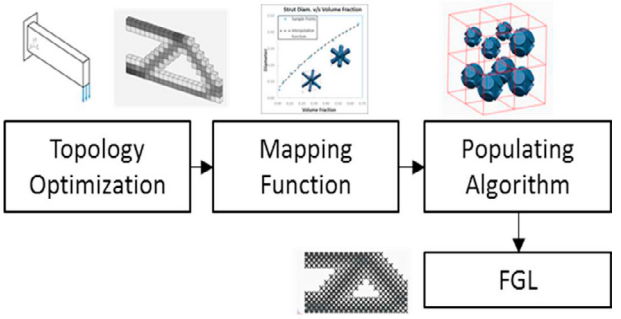

Fig. 5. Sequence of steps adopted in this work to develop FGLs using B-spline surface-based BCC lattices.

of volume occupied by the unit cell to that of the complete voxel. A mapping scheme is used to map this voxelized distributions of volume fractions to corresponding geometric parameters of the unit cells. An appropriate algorithm is required to systematically fill the voxelized design space with those unit cells to get the desired structure. Finally, post-processing steps such as trimming operations might be required to refine the structure. Starting from the mapping methodology, different steps involved in generating the FGLs are discussed in subsequent sections.

3.3. Mapping scheme

In this work, the volume fraction of the unit cell is controlled by changing the unit cell strut diameter. Therefore, a scheme is required that can map different volume fractions from SIMP output to corresponding strut diameters of each unit cell. To achieve this mapping, samples of B-spline surface-based unit cells were created with different strut diameters and their corresponding volume fractions were also tabulated. The volume fractions were obtained by using the inbuilt APIs inside the SIEMENS NX Open programming framework. Using these sample points, a simple quadratic curve (Fig. 6) is fit that gives

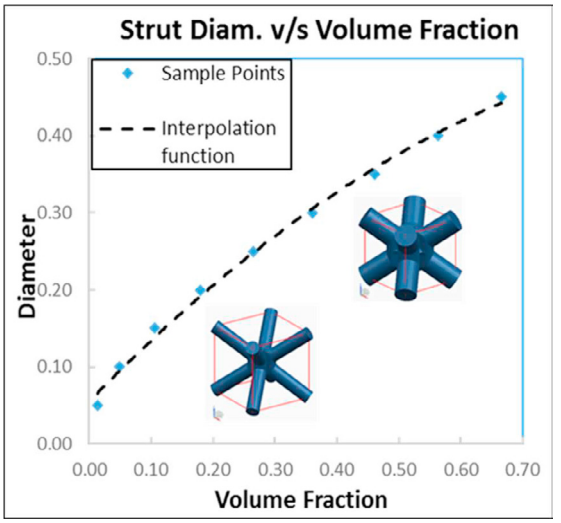

Fig. 6. Fitted function to obtain mapping between volume fractions and strut diameters.

strut diameters as a function of volume fractions for each unit cell.

3.4. Populating algorithm

Existing design methodologies for generating a BCC lattice structure generate a structure as shown in Fig. 7. The severity of connectivity issue is evident when struts corresponding to unit cells of different volume fractions merge at one point. Such

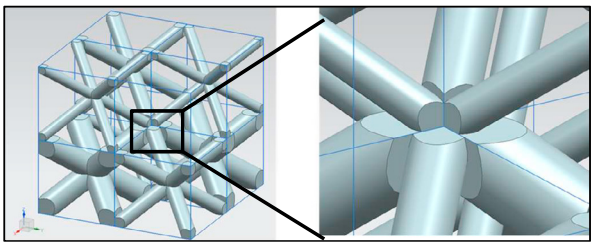

Fig. 7. Connectivity problem with conventional design method

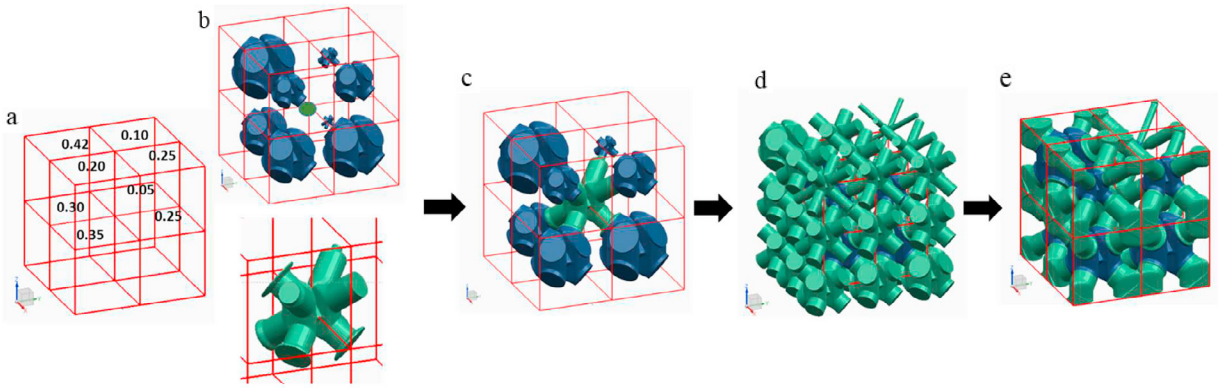

Fig. 8. (a) A 2 by 2 by 2 voxel grid with different volume fractions; (b) connecting cells in green and central unit cells in blue. Position of one connecting unit cell is highlighted with a green circle in the top picture. Connections of both the cell types is shown in (c); full lattice structure developed is shown in (d) and the refined structure after trimming of struts along the 6 boundary faces is shown in (e).

design is not desired and leads to undesired mechanical behavior [2].

To address this issue, in this paper a new approach has been defined where two types of unit cells are used, termed as central unit cell and connecting unit cell as shown in Fig. 8(b). The central unit cells sit at the center of each voxel and connecting unit cells occupy all the corners with their centers coinciding with voxel centers as shown in Fig. 8(b). Each corner unit cell is used to establish connectivity between the central unit cells of different densities that occupy the voxels sharing that corner point.

The central unit cell is created with strut diameter value derived from volume fraction mapping function and its cell size is same as the voxel size in the previous step of topology optimization. The strut diameter for the connecting unit cell is calculated by taking the average of the diameters of the available nearest neighboring unit cells. There could be a maximum of 8 neighbors and a minimum of 1. In the absence of all 8 neighbors the strut diameters of non-existing unit cells are ignored for calculating the average diameter of the corner unit cell. The starting point of all the struts of central unit cells is at a small distance from the end-point along the skeletal curve instead of the voxel's corners as shown in Fig. 1(a). The ends of each of the struts of a connecting unit cell are constrained to join the strut ends of the corresponding central unit cell. This, however, could make the struts of the connecting unit cells to be of different lengths. In order to maintain a G1 continuity at strut-strut meeting point, the cross-section of the last two strut polygons of connecting unit cell is of exactly the same size as that of the strut polygon of the central unit cell strut polygons (Fig. 9). This local shape modification could be possible because of the flexibility allowed by the B-spline surfaces.

Once all unit cells are generated, the FGL is in the form of multiple solid bodies (unit cells). To unite the model, a simple Boolean unite operation can be performed using the Graphic User Interface (GUI) of the CAD software. The redundant struts of the connecting unit cells at the boundaries with no central unit cell to attach to, could be trimmed off since they contribute extra weight to the whole structure.

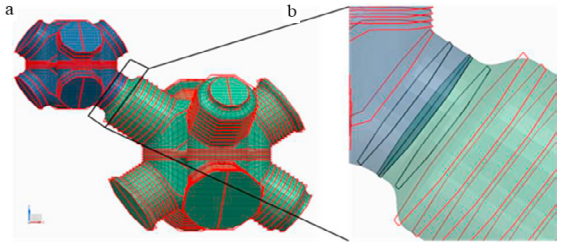

Fig. 9. Constraining connecting unit cell to join with central unit cells with G^1 continuity by making the first two strut polygons (in black) of same diameter for both struts. All other control polygons are shown in red.

4. Example problems

Developing FGLs for achieving weight reduction while maximizing stiffness has attracted a lot of interest in the recent studies by [5, 23, 24]. However, it is challenging to design FGLs using truss type lattices due to inability to ensure connectivity across unit cells of varying volume fractions [9]. Although a similar light-weighting can be achieved by using a uniform density filling but the structural performance is compromised in comparison to FGLs [24].

Two examples are discussed where the methodology discussed in this paper is used to create BCC unit cell based FGLs to maximize the overall stiffness. Enlarged views (Fig. 11 and Fig. 14) of sample zones of the developed 3D FGL structures are also shown for each example. It can be seen that the struts don't mash into each other at intersection zones and the variation in strut diameter across different volume fractions is adjusted for at the strut ends of connecting unit cells (Fig. 11(b) and Fig. 14 (b)). Structures with uniform distribution of density are also created with BCC unit cells, and both are compared for stiffness values by performing Finite Element Analysis (FEA). The structures are meshed and analyzed using Altair Hypermesh and Optistruct software. The results confirm that the resulting FGLs performs better on stiffness than uniform density structures. Hence, the above discussed methodology could be useful in enabling designers to create FGLs for optimal performance.

4.1. Simple cantilever beam

A simple cantilever beam with one end fixed and load applied on the lower free edge is used for the first example as shown in Fig. 10(a). It is voxelized into cubic voxels of 1 mm side length. The beam is 20 mm long, 10 mm in height and 1 mm wide. For generating the graded structure (Fig. 10(c)), the maximum possible volume fraction of each voxel is set to 62% and the minimum volume fraction is set to 20% to obtain a net volume fraction of 32.51% after trimming the redundant struts at the boundary. Another cantilever beam design was obtained

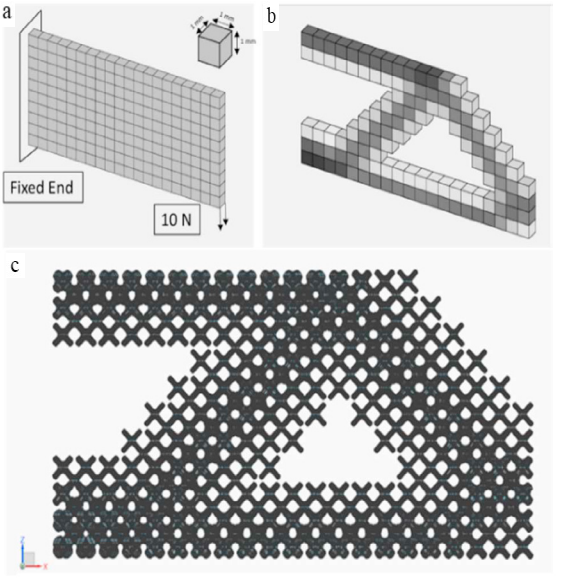

Fig. 10. (a) Voxelized cantilever beam; (b) topologically optimized beam in (b); (c) BCC based FGL generated using B-spline surfaces.

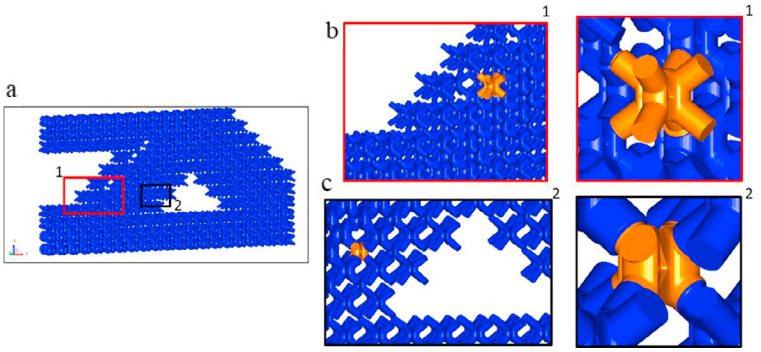

Fig. 11. Joints of connecting and central unit cells. (a) shows another view of the full graded structure. (b) snapshot and magnified picture of a connecting unit cell in the red view block of (a). (c) snapshot and magnified picture of a central unit cell in the black view block of (a). There is another unit cell attached to the free strut end visible in the picture 2, it is hidden for getting a clear snapshot.

by filling with BCC unit cells of equivalent constant volume fraction.

Table 1. Design parameters for example 1.

Design Parameters	Values
Length (mm)	20
Width (mm)	1
Height (mm)	10
Young's Modulus (MPa)	2.10E4
Poisson's ratio	0.3
Load (N)	10
Unit Cell Size (mm)	1

The loading conditions are summarized in Table 1., the FEA results are summarized in Table 2 and shown in Fig. 12. The results validate that the B-spline surface-based methodology could enable creation of optimized cantilever beam that has a displacement much smaller than the uniform density lattice structure with comparable values of the maximum Von-Mises stresses.

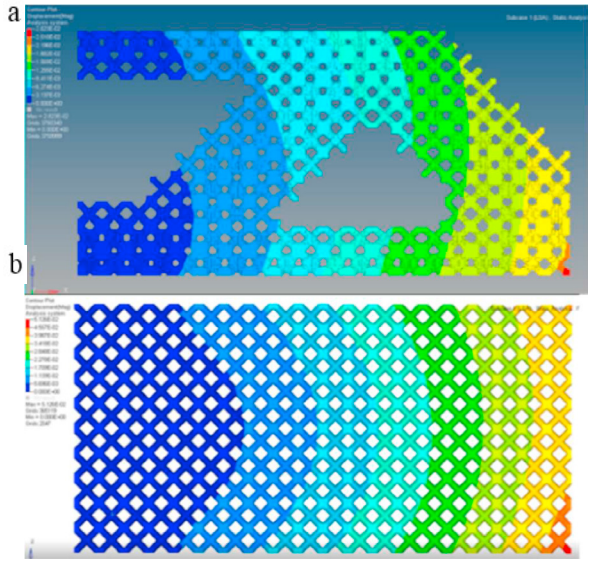

Fig. 12. Displacement results for uniform and graded lattice structure

Table 2. Results for the simple cantilever beam.

Parameters	Uniform Density Beam	FGL Beam
Volume Fraction	32.61%	32.51%
Max Displacement Magnitude (mm)	5.12 E-2	2.82 E-2
Max Von-Mises Stress (MPa)	8.166 E2	9.66 E2

4.2. Cantilever beam with hole

The second test case is a cantilever beam with a polygonal hole as shown in Fig. 13. It is 25 mm in length, 10 mm in height and 1 mm in width with one end fixed and a 10 N load on the lower edge. There are two cases discussed, first is comparison with the beam geometry filled with lattices of uniform density. The second case is also filled with unit cells of uniform volume fraction, but in an optimized topology of the beam. Similar to the example 1, for the graded structure (Fig. 13(c)), the maximum possible volume fraction of each voxel is set to 62% and the minimum volume fraction is set to 20%. The loading parameters are summarized in Table 3. The enlarged views of

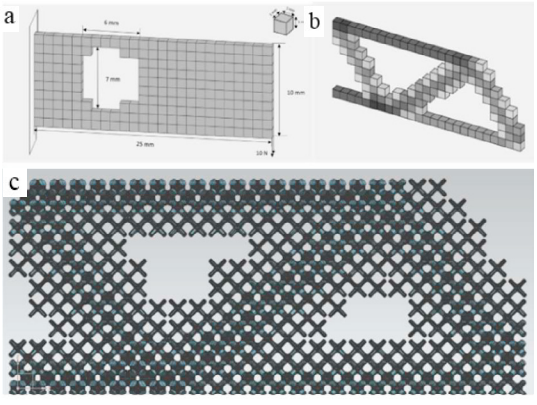

Fig. 13. (a) Voxelized cantilever beam; topologically optimized beam in (b); BCC based FGL generated using B-spline surfaces in (c).

different sections of the developed FGL are also shown in Fig. 14.

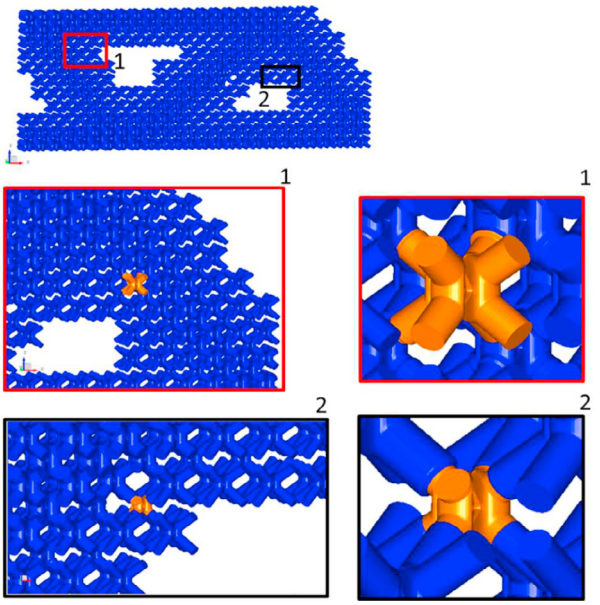

Fig. 14. Joints of connecting and central unit cells. (a) shows another view of the full graded structure. (b) snapshot and magnified picture of a connecting unit cell in the red view block of (a). (c) snapshot and magnified picture of a central unit cell in the black view block of (a). There is another unit cell attached to the free strut end visible in the picture 2, it is hidden for getting a clear snapshot.

Table 3. Design parameters for cantilever beam with hole.

Design Parameters	Values
Length (mm)	25
Width (mm)	1
Height (mm)	10
Young's Modulus (MPa)	2.10E4
Poisson's Ratio	0.3
Load (N)	10
Unit Cell Size (mm)	1

4.2.1. Comparison with uniformly filled lattice structure of the beam

A 35.5% overall volume fraction obtained was obtained for of the FGL after trimming of the redundant struts at the boundary. The structure was compared to a heavier uniform density lattice structure with 38.5% overall volume fraction. A cubic voxel size of 1 mm was used in both the cases. Table 4 shows the displacement results for B-spline based FGLs and uniform density lattice structures. The FGL exhibits a much higher stiffness while being 7.8% lighter than the lattice structure with a uniform fill. The Von-Mises stress values of the FGL are slightly higher due to the lower volume fraction of the FGL in comparison to the uniform density beam. More material addition in the FGL to compensate for higher stress would lead to a decrease in light-weighting.

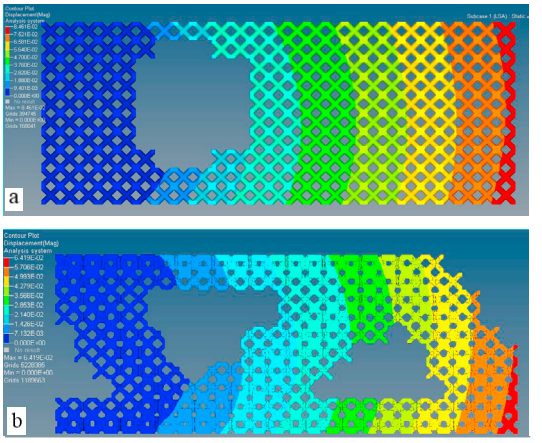

Fig. 15. Displacement results for uniform and graded lattice structure

Table 4. Results for cantilever beam with hole.

Parameters	Uniform Density Beam	FGL Beam
Volume Fraction	38.51%	35.50%
Max Displacement Magnitude (mm)	8.47 E-2	6.41 E-2
Max Von-Mises Stress (MPa)	5.86 E2	7.0 E2

4.2.2. Comparison with topologically optimized beam having regular BCC unit cells

Another method to avoid the problem of connectivity across unit cells of different volume fractions for obtaining lattice structures with higher stiffness is to populate a topologically optimized structure with unit cells of uniform density as reported in [5]. A structure (Fig. 16) was generated using the topology optimized output of geometry in the previous

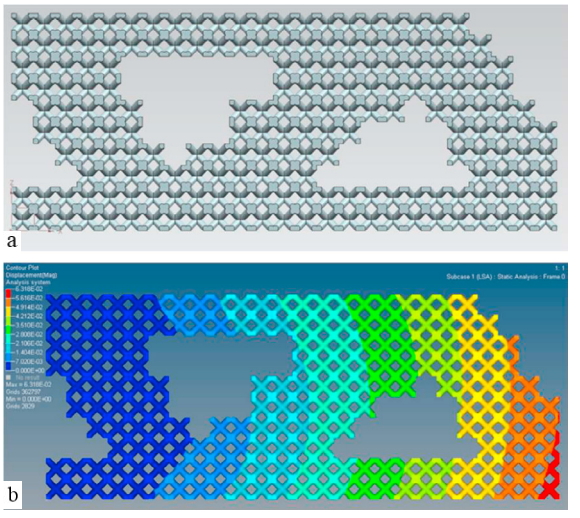

Fig. 16. (a) CAD design of topology optimized structure from example 2 populated with regular BCC unit cells with uniform density fill. (b) displacement results for same loading conditions as in example 2.

example using the design parameters in Table 3, and all the voxels were populated with regular BCC unit cells of uniform volume fraction. The volume fraction of each unit cell is evaluated such that the overall volume fraction of the structure is 35.85%. Table 5 shows that for a similar value of the overall volume fraction, the stiffness value of the FGL is comparable to this structure though both the structures are stiffer than the uniformly filled beam in Fig. 15(a). This shows that topology optimization plays a key role in maximizing the stiffness. However, when a graded distribution of lattice is required in advanced applications such as development of graded porous structure of bones [2], the FGL design methodology could be useful to develop stiffer structures.

Table 5. Results for topology optimized beam with uniform density fill

Parameters	Optimized Beam with uniform density fill	FGL Beam
Volume Fraction	35.85%	35.50%
Max Displacement Magnitude (mm)	6.31 E-2	6.41 E-2
Max Von-Mises Stress (MPa)	7.50 E2	7 E2

5. Conclusion

A new B-spline surface-based methodology to develop smoothly connected FGLs with strut type unit cells was discussed in this paper. The approach for a multi-furcation geometry in the case of a BCC unit cell was extended from the lead author's previous work on bifurcating geometries in [1]. It was shown that using a 3rd order B-spline surfaces allow flexibility to alter the geometry of the unit cell locally to meet connectivity requirements in a 3D graded lattice structure. Two type of unit cells were developed – central and connecting cells that were mapped systematically onto the density distribution obtained from a topology optimization routine. Using FGLs is advantageous since they are designed to perform optimally while being light-weighted. The open porous architecture also provides the design opportunity for imparting additional functionalities in a structure such as convective heat transfer by flow of a coolant through the pores. This methodology provides designers with a new tool that now enables designing robust FGLs for designing optimal structures which could then be manufactured by leveraging AM technologies. However, to ensure robust manufacturability with AM technologies such as the DMLS process, DFAM parameters such as compensating strut diameters, pore size and small openings are required to be taken into consideration in the proposed methodology.

In the absence of tools to generate FGLs that take advantage of porous architecture of lattices, a viable alternative is to use uniform density filling especially in the case of strut type lattice such as BCC. However, previous researches have shown that FGLs perform better on stiffness criteria than uniform density lattice structures. Examples were discussed where FGLs designed using the methodology discussed in this paper were compared with uniform density lattice structures of equivalent or greater overall volume fraction. The results confirm the applicability of the method to design graded lattice structures with high stiffness using strut type lattices. The method could therefore be advantageous to design graded density distribution of lattices in additive manufacturing based medical applications.

6. Future Scope

The methodology discussed in this paper is presented only for the case of a BCC unit cell. With some modifications the idea could be extended to other strut type unit cells geometries where connectivity could be an issue. The manual trim operations for redundant struts could be avoided by improving the unit cell design algorithm to be able to generate a watertight representation of connecting unit cells at the boundary of design space. This could lead to significant savings on post-processing time. The next step in this work is including DFAM parameters and constraints in this methodology to ensure that the designed FGLs are not only robust but easier to build as well with AM technologies.

7. Acknowledgement

The algorithms were implemented in SIEMENS NX software and the authors would like to acknowledge SIEMENS for providing the software tool and support for this academic research.

References

[1] Bhatt A D, Goel A, Gupta U and Awasthi S, Reconstruction of Branched Surfaces: Experiments with Disjoint B-spline Surface, Computer-Aided Design and Applications, 12 (2015) 76-85.

[2] Han C, Li Y, Wang Q, Wen S, Wei Q, Yan C, Hao L, Liu J and Shi Y, Continuous functionally graded porous titanium scaffolds manufactured by selective laser melting for bone implants, Journal of the Mechanical Behavior of Biomedical Materials 80 (2018) 119-127.

[3] Dumas M, Terriault P and Brailovski V, Modelling and characterization of a porosity graded lattice structure for additively manufactured biomaterials, Mater Des 121 (2017) 383-392.

[4] Maloney K J, Fink K D, Schaedler T A, Kolodziejska J A, Jacobsen A J and Roper C S, Multifunctional heat exchangers derived from three-dimensional micro-lattice structures, Int. J. Heat Mass Transfer, 55 (2012) 2486-2493.

[5] Wang Y, Zhang L, Daynes S, Zhang H, Feih S and Wang M Y, Design of graded lattice structure with optimized mesostructures for additive manufacturing, Mater Des,142 (2018) 114-123.

[6] Maskery I, Hussey A, Panesar A, Aremu A, Tuck C, Ashcroft I and Hague R, An investigation into reinforced and functionally graded lattice structures, Journal of Cellular Plastics, 53 (2017) 151-165.

[7] Liu K and Tovar A, An efficient 3D topology optimization code written in Matlab, Structural and Multidisciplinary Optimization, 50 (2014) 1175-1196.

[8] Panesar A, Abdi M, Hickman D and Ashcroft I, Strategies for functionally graded lattice structures derived using topology optimisation for additive manufacturing, Additive Manufacturing, 19, (2018) 81-94.

[9] Zhang B, Mhapsekar K and Anand S, Design of variable-density structures for additive manufacturing using gyroid lattices, in: ASME 2017 International Design Engineering Technical Conferences and Computers and Information in Engineering Conference, 2017, pp. V004T05A015-V004T05A015.

[10] Arisoy E B, Musuvathy S, Mirabella L and Slavin E, Design and topology optimization of lattice structures using deformable implicit surfaces for additive manufacturing, in: ASME 2015 International Design Engineering Technical Conferences and Computers and Information in Engineering Conference, 2015, pp. V004T05A003-V004T05A003.

[11] Wang H, Chen Y and Rosen D W, A hybrid geometric modeling method for large scale conformal cellular structures, in: ASME Computers and Information in Engineering Conference, Long Beach, CA, Sept, 2005, pp. 24-28.

[12] Chen Y, A mesh-based geometric modeling method for general structures, in: ASME International Design Engineering Technical Conferences and Computers and Information in Engineering Conferences, Philadelphia, PA, 2006, pp. 269-281.

[13] McMillan M, Jurg M, Leary M and Brandt M, Programmatic lattice generation for additive manufacture, Procedia Technology, 20 (2015) 178-184.

[14] Savio G, Meneghello R and Concheri G, Geometric modeling of lattice structures for additive manufacturing, Rapid Prototyping Journal, 24 (2018) 351-360.

[15] Kou S and Tan S, An approach of irregular porous structure modeling based on subdivision and NURBS, Computer-Aided Design and Applications, 10 (2013) 355-369.

[16] Raymont D R, On the generation and characterisation of internal micro-architectures, 2011.

[17] Yoo D J, Porous scaffold design using the distance field and triply periodic minimal surface models, Biomaterials, 32 (2011) 7741-7754.

[18] Arabnejad S, Johnston R B, Pura J A, Singh B, Tanzer M and Pasini D, High-strength porous biomaterials for bone replacement: A strategy to assess the interplay between cell morphology, mechanical properties, bone ingrowth and manufacturing constraints, Acta Biomaterialia, 30 (2016) 345-356.

[19] Aremu A, Brennan-Craddock J, Panesar A, Ashcroft I, Hague R J, Wildman R D and Tuck C, A voxel-based method of constructing and skinning conformal and functionally graded lattice structures suitable for additive manufacturing, Additive Manufacturing, 13 (2017) 1-13.

[20] Bendsøe M P and Kikuchi N, Generating optimal topologies in structural design using a homogenization method, Comput. Methods Appl. Mech. Eng., 71 (1988) 197-224.

[21] Bendsøe M P and Sigmund O, Material interpolation schemes in topology optimization, Arch Appl Mech, 69 (1999) 635-654.

[22] David F R and Adams J A, Mathematical elements for computer graphics, New Delhi, Tata McGraw-Hill, 2002.

[23] Zhang P, Toman J, Yu Y, Biyikli E, Kirca M, Chmielus M and To A C, Efficient design-optimization of variable-density hexagonal cellular structure by additive manufacturing: theory and validation, Journal of Manufacturing Science and Engineering, 137 (2015) 021004.

[24] Cheng L, Zhang P, Biyikli E, Bai J, Pilz S and To A C, Integration of topology optimization with efficient design of additive manufactured cellular structures, in: Solid Freeform Fabrication Symposium, 2015, pp. 1370-1377.